Perturbed ion traps: A generalization of the three-dimensional Hénon–Heiles problem

V. Lanchares[a] and A. I. Pascual
Departamento de Matemáticas y Computación, Universidad de La Rioja, 26004 Logroño, Spain

J. Palacián and P. Yanguas
Departamento de Matemática e Informática, Universidad Pública de Navarra, 31006 Pamplona, Spain

J. P. Salas
Area de Física Aplicada, Universidad de La Rioja, 26004 Logroño, Spain

(Received 12 July 2001; accepted 13 December 2001; published 21 February 2002)

This paper presents an analytical study of an axially symmetric perturbation of the Penning trap. This system is modeled as a generalization of the three-dimensional (3D) Hénon–Heiles potential. Thus, the same techniques which succeeded in the study of the 3D Hénon–Heiles system apply here. The departure Hamiltonian is three dimensional, although it possesses an axial symmetry. This property, together with an averaging process, is used to reduce the original system to an integrable one. We study the flow of the reduced Hamiltonian: equilibria, bifurcations, and stability, extracting thereafter the relevant information about the dynamics of the original problem. © *2002 American Institute of Physics.* [DOI: 10.1063/1.1449957]

Since the beginning of the last century, the effect of the application of external fields to atoms has played a crucial role in the development of atomic physics. In particular, the application of static electric and magnetic fields to create trapping phenomena is a remarkable feature. When the trapped particle is an ion, lab experiments are used to perform very precise spectroscopic measurements and to construct accurate atomic clocks. In this paper we focus on one of these experiments: the Penning trap, which is described in Sec. I. Due to physical imperfections of the real experiment, some perturbations have to be added to the original model. The system we consider is a three-dimensional (3D) Hamiltonian composed of the main part (a 3D harmonic oscillator with two equal frequencies) plus a small perturbation composed of cubic terms. Hence, the model is ideal to be considered from an analytical point of view within the framework of perturbation theory. Our goal is to perform a qualitative analysis of the effect caused by the imperfections on the Penning trap. Taking into account the axial symmetry of the problem and by means of an averaging process, we arrive to a one degree of freedom system. A global analysis of the phase flow of this reduced system indicates that one of the control parameters involved in the design of the Penning trap serves to attenuate the nonlinear behavior.

I. INTRODUCTION

As is known, one of the most celebrated models in nonlinear physics has been the perturbed harmonic oscillator. One reason is that its apparently deceptive simplicity hides a rich nonlinear behavior which converts this system to a trial field where it is possible to test the modern theories on dynamical systems. Moreover, its experimental and theoretical applicability runs over a wide and disparate fields, such as dynamical astronomy, see Refs. 1, 2, 3, particle and plasma physics, see Refs. 4, 5 or atomic physics, see Refs. 6, 7. In particular, the Penning ion trap (in Refs. 8–10) stands out because it is one of the most useful models in atomic physics.

Briefly described, the Penning trap represents a three-dimensional (3D) trapping of a charge or ion due to an axially symmetric (''*perfect*'') quadrupole electric field plus a static magnetic field. The perfect quadrupole electric potential is achieved by means of a set of three electrodes. One of the electrodes, called the ring, is shaped like the inner surface of a toroid. The other two are like hemispheres placed above and below the ring. In this arrangement, the quadrupole potential acts as a trap only in the direction of the axis between the hemispheres (we call this axis z), while the motion in the radial plane (Oxy plane) is unstable. The presence of the magnetic field along the z axis provides the complete trapping and the motion of the ion remains harmonic.

In the above-mentioned ideal configuration, the Penning trap is modeled by means of an unperturbed three-dimensional harmonic oscillator (as can be seen in Refs. 8, 9). However, electrostatic field perturbations may arise from imperfections in the physical design of the electrodes, as well as from misalignments in the experimental setup, see for instance Refs. 10–12. We can separate these perturbations into harmonic and anharmonic perturbations. In particular, the second group is the most interesting one because it leads to nonlinear motion.

As we will see in Sec. II, from the point of view of nonlinear dynamics, the Hamiltonian describing the perturbed Penning trap can be considered as a very general extension of the famous Hénon–Heiles model, see Ref. 13. Then, the real physical system studied in this paper is a good

[a]Electronic mail: victor.lanchares@dmc.unirioja.es

candidate to apply the nonlinear dynamics techniques. However, despite the plethora of works dealing with the two-dimensional (2D) Hénon–Heiles model (see Ref. 7 for a review), a general theoretical study of the perturbed Penning trap is almost an impossible task. Hence, in this paper we only consider axially symmetric perturbations of the three-dimensional Penning trap, which is also axially symmetric. In this way we take advantage of the symmetric character of the 3D perturbed system to reduce it to one of dimension two. In particular, we will treat the *sextupolar* perturbation.

The study is performed from an analytical point of view. We consider the Hamiltonian representing the perturbed Penning trap as a sum of an unperturbed part, the corresponding harmonic oscillator, and the perturbation associated with the axially symmetric electrostatic imperfection. The basic idea is to transform this system into an equivalent integrable Hamiltonian easier to be studied and containing the main features of the original system. Thus, we can extract dynamical information of the original system from the integrable Hamiltonian.

We construct this new system in two steps: first we apply an asymptotic transformation based on the Lie–Deprit method, see Ref. 14. Fixing a value for the energy, the transformed, i.e., normalized, system is of two degrees of freedom. The reduced phase space for the isotropic harmonic oscillator is the *complex projective* space CP^2. Second, we reduce the axial symmetry and fix a value for the new formal integral, the third component of the angular momentum vector. After this process, the twice reduced system is of one degree of freedom (integrable). Then we analyze the dynamical features of this system, calculating its equilibria and three types of bifurcation lines: saddle center, Hamiltonian Hopf, and Hamiltonian flip. An estimation of the error committed in the Lie transformation allows us to conclude that our approach is valid in a neighborhood of the origin. This is reinforced numerically using some Poincaré surfaces of section. Therefore using KAM theory, we infer that the bifurcations of the relative equilibria correspond to bifurcations of 2D invariant tori and quasiperiodic orbits of the original Hamiltonian. In the end all these mathematical considerations permit are to establish some relevant physical aspects of the perturbed Penning trap.

The paper is structured as follows: in Sec. II we formulate the problem. In Sec. III we describe and perform the reduction. Once the integrable Hamiltonian has been determined, we study the normalized dynamics in Sec. IV. This involves the determination of equilibria and bifurcations with the corresponding analysis of the stability. In Sec. V we describe the phase flow evolution. Finally, in Sec. VI we establish the connection between the reduced and the original systems and present the conclusions in Sec. VII.

II. THE PERTURBED PENNING TRAP

The Hamiltonian for a single ion of mass m and charge q trapped in a *perfect* Penning trap is given by

$$\mathcal{H}=\frac{1}{2m}(p_x^2+p_y^2+p_z^2)+w_L(xp_y-yp_x)+\frac{m}{2}\left(w_L^2-\frac{w_z^2}{2}\right)\times(x^2+y^2)+\frac{m}{2}w_z^2z^2, \tag{1}$$

where w_z and w_L are, respectively, the frequency induced by the quadrupole electric field and the Larmor frequency, see Ref. 12. The trapping condition is achieved when $w^2=w_L^2-w_z^2/2\geqslant 0$, which ensures a stable motion in the radial plane. However, the perfect Penning trap is not a realistic model due to the imperfections of the electric field. In this way, the potential induced by the quadrupole electric field, that is

$$V=\frac{w_z^2}{4}(2z^2-x^2-y^2),$$

is substituted, as in Refs. 12 and 15, by the multipole expansion of the electrostatic potential. This expansion in spherical coordinates $(r,\ \theta,\ \phi)$ takes the form

$$V=\sum_{l\geqslant 0} V_l,$$

where

$$V_l=\sum_{k=0}^{l} a_{l,k}r^l\mathcal{P}_l^k(\cos\theta)\cos(k\phi), \tag{2}$$

$\mathcal{P}_l^k$ being the Legendre functions. The term $V_0=a_{0,0}$ defines the origin of the electrostatic potential. The linear term $V_1=a_{1,0}\ z+a_{1,1}x$ gives rise to a constant force and can be dropped. Hence, the Hamiltonian of the perturbed Penning trap (in Cartesian coordinates) is

$$\mathcal{H}=\frac{1}{2m}(p_x^2+p_y^2+p_z^2)+w_LL_z+\frac{m}{2}w_L^2(x^2+y^2)+\sum_{l\leqslant 2} V_l, \tag{3}$$

where $L_z=xp_y-yp_x$ is the z component of the angular momentum.

In general, Hamiltonian (3) represents a three-dimensional dynamical system. However, by assuming z-axial symmetry, it is possible to lower the dimension of the problem, as L_z is a constant of motion. Under this assumption all $a_{l,k}$ terms in Eq. (3) with $k\neq 0$ are zero. Now, this Hamilton function defines a two-degree-of-freedom dynamical system. At this point we take V_2 and V_3 (with $a_{l,k}=0$ if $k>0$), which are, respectively, the (perfect) quadrupole and the sextupole terms. The corresponding Hamiltonian yields

$$\mathcal{H}=\frac{1}{2m}(p_x^2+p_y^2+p_z^2)+w_LL_z+\frac{m}{2}w_L^2(x^2+y^2)+\frac{a_{2,0}}{2}(2z^2-x^2-y^2)+\frac{a_{3,0}}{2}z(2z^2-3x^2-3y^2). \tag{4}$$

The parameter $a_{2,0}$ has dimensions of mass over time square so that it introduces a frequency w_z in such a way that $a_{2,0}=mw_z^2/2$. In order to simplify notation, we rewrite the sex-

tupole parameter $\frac{1}{2}a_{3,0}$ as a_3 and we assume the mass m equal to one. With this new notation, Hamiltonian (4) takes the form

$$\mathcal{H}=\tfrac{1}{2}(p_x^2+p_y^2+p_z^2)+w_L L_z+\tfrac{1}{2}w^2(x^2+y^2)+\tfrac{1}{2}w_z^2 z^2 + a_3 z(2z^2-3x^2-3y^2), \tag{5}$$

where we are assuming the trapping condition $w^2=w_L^2 - w_z^2/2\geqslant 0$.

As we pointed out in Sec. I, owing to the cylindrical symmetry of the system, it is possible to eliminate the linear term $w_L\, L_z$ in Eq. (5) by expressing the Hamiltonian in a reference frame (x',y',z'') rotating with the frequency w_L around the z axis. This canonical transformation is given by the generating function

$$W=p_x'(x\cos w_L t+y\sin w_L t) + p_y'(-x\sin w_L t+y\cos w_L t)+p_z',$$

where

$$p_x=\frac{\partial W}{\partial x},\quad p_y=\frac{\partial W}{\partial y},\quad p_z=\frac{\partial W}{\partial z},$$

$$x'=\frac{\partial W}{\partial p_{x'}},\quad y'=\frac{\partial W}{\partial p_{y'}},\quad z'=\frac{\partial W}{\partial p_{z'}}.$$

The new Hamiltonian is given by

$$\mathcal{H}'=\mathcal{H}+\frac{\partial W}{\partial t},$$

which results to be, after dropping the primes,

$$\mathcal{H}=\tfrac{1}{2}(p_x^2+p_y^2+p_z^2)+\tfrac{1}{2}w^2(x^2+y^2)+\tfrac{1}{2}w_z^2 z^2 + a_3 z(2z^2-3x^2-3y^2), \tag{6}$$

and Eq. (6) represents a three-dimensional perturbed $w{:}w{:}w_z$ harmonic oscillator.

We note that in the particular situation $w_z=w$ (the isotropic case), Hamiltonian (6) corresponds to the Hénon–Heiles system in three dimensions. Hence, we can consider Eq. (6) as a more general Hénon–Heiles system in three dimensions, see Refs. 16 and 17. Thus, we name the system described by Hamiltonian (6) the axially symmetric perturbed *generalized 3D Hénon–Heiles system*.

III. NORMALIZATION AND REDUCTION

Our aim in this section is to simplify $\mathcal{H}$. With this purpose we perform an asymptotic transformation up to second order of approximation. The transformation is constructed in such a way that we average the original system over one of the angles. Indeed, the high-order averaging procedure can be interpreted as a normalization technique since the ''elimination'' of an angle variable is completely equivalent to the construction of a formal integral, see for instance Ref. 18. At this point we want to emphasize that these types of transformations are, in general, divergent. However, one can still build approximations to the original problem (e.g., normalized or averaged Hamilton functions) good enough to be useful for analytical purposes. This must be accompanied by an estimate of the error made after truncation of the high-order terms.

By assuming the sextupole parameter a_3 small, we can consider the system defined by Hamiltonian (6) as a weakly perturbed $w{:}w{:}w_z$ harmonic oscillator. When $w_z\neq w$, in order to still consider Eq. (6) as a weakly perturbed isotropic oscillator, we will assume $w_z\approx w$. This allows us to define a small detuning parameter $|\delta|\ll 1$ in such a way that it is possible to split $w_z^2=w^2+\delta w^2$. Therefore, Hamiltonian (6) becomes

$$\mathcal{H}=\mathcal{H}_0+\mathcal{H}_1,$$

$$\mathcal{H}_0=\tfrac{1}{2}(p_x^2+p_y^2+p_z^2)+\tfrac{1}{2}w^2(x^2+y^2+z^2), \tag{7}$$

$$\mathcal{H}_1=\tfrac{1}{2}\delta w^2 z^2+a_3 z(2z^2-3x^2-3y^2),$$

where $\mathcal{H}_1$ is the perturbation to $\mathcal{H}_0$.

The goal of this section is to reduce the three-degree-of-freedom Hamiltonian $\mathcal{H}$ to a simpler one, but preserving the main features of the original system. First of all, we normalize system (7). In this way we obtain a two-degree-of-freedom Hamiltonian. Fixing a value for the energy, $\mathcal{H}=h$, we pass from the original six-dimensional phase space, $\mathbf{R}^6$, to the reduced one: the four-dimensional complex projective space $\mathbf{CP}^2$. It is parametrized by nine linearly independent generators, for example, see Ref. 16. Moreover, let us note that both $\mathcal{H}_0$ and $\mathcal{H}_1$ are axially symmetric. Thus, a second reduction can be carried out so as to obtain a one-degree-of-freedom reduced system. In this case, the second reduced space is a semialgebraic variety of dimension two. This (second) reduced space is generated by five linearly independent polynomials, details appear in Ref. 19. In the subsequent paragraphs we develop these two reductions.

The normalization procedure is carried out by means of Lie transformations following the Lie–Deprit method, see Ref. 14. We use nodal-Lissajous variables, a set of action-angle variables which describe particularly well axially symmetric perturbations of oscillators in 1–1–1 resonance, see Ref. 20.

Since the solutions of perturbed oscillators in 1–1–1 resonance are perturbed ellipses, nodal-Lissajous variables allow one to describe the trajectories easily. The set is given by (l, g, ν, L, G, N), where l stands for the elliptic anomaly and describes the position of the particle in a trajectory from the semiminor axis. The angles g and ν are called, respectively, the argument of perigee and the argument of the node. Both give the position of the perturbed ellipse in the space since, on the one hand, g measures the position of the semiminor axis, reckoned from the nodal line, while ν goes from the nodal line to the orbital plane. The momentum L is the action associated to l and is related to the energy of the unperturbed system $\mathcal{H}_0$. Besides, G represents the modulus of the angular momentum vector $\mathbf{G}$ of the problem, while $N(\equiv L_z)$ refers to the third component of $\mathbf{G}$. One important feature of these variables is precisely that the third component and the modulus of the angular momentum are among the conjugate moments. This makes it possible to understand the effects of the perturbations on the unperturbed ellipses as

the variations of their inclinations and eccentricities. The set of nodal-Lissajous variables is defined in the domain $\Delta \subset \mathbf{R}^6$ such that

$$\Delta = [0,2\pi)\times[0,2\pi)\times[0,2\pi)\times\{L>0\} \times\{0<G<L\}\times\{|N|<G\}.$$

Thus, circular ($G=L$), rectilinear ($G=0$), and equatorial trajectories ($G=|N|$) are excluded from the domain. For the explicit expressions of Cartesian variables as functions of nodal-Lissajous variables, and a more detailed description of them, the reader is referred to Refs. 20 and 21.

In this way, the expression of $\mathcal{H}_0$ in nodal-Lissajous variables is proportional to the action L. Thence, normalizing in nodal-Lissajous means ''eliminating the variable l'' up to a certain order, obtaining an averaged orbit with respect to the elliptic anomaly. As l represents time, it varies quickly and we ''eliminate'' it because we are not interested in the position of the particle in each moment, but in the evolution of the orbit at a large time scale.

The transformation up to order M is a change of variables $\Psi:(l',g',\nu',L',G',N')\to(l,g,\nu,L,G,N)$ whose goal is to transform the Hamiltonian

$$\mathcal{H}(l,g,\nu,L,G,N;\epsilon)=\sum_{n\geqslant 0}\frac{\epsilon^n}{n!}\mathcal{H}_n(l,g,\nu,L,G,N),$$

into the new Hamiltonian

$$\mathcal{K}(l',g',\nu',L',G',N';\epsilon) =\sum_{n\geqslant 0}^{M}\frac{\epsilon^n}{n!}\mathcal{K}_n(-,g',\nu',L',G',N')+\mathcal{O}(\epsilon^{M+1}),$$

through a generating function

$$\mathcal{W}(l,g,\nu,L,G,N;\epsilon)=\sum_{n\geqslant 1}^{M}\frac{\epsilon^n}{n!}\mathcal{W}_n(l,g,\nu,L,G,N).$$

Parameter ϵ is a small dimensionless quantity. The construction of $\mathcal{K}$, or averaged normalized Hamiltonian, is performed step by step. We first identify $\mathcal{H}_0\equiv\mathcal{K}_0$. Then, at each step $n>0$ of the procedure we have to solve the homology equation

$$\{\mathcal{W}_n,\mathcal{H}_0\}+\mathcal{K}_n=\tilde{\mathcal{H}}_{0n},$$

where $\tilde{\mathcal{H}}_{0n}$ collects all the terms known from the previous order and $\{\cdot,\cdot\}$ represents the standard Poisson bracket. The solution of this equation is simply an average with respect to the elliptic anomaly:

$$\mathcal{K}_n=(2\pi)^{-1}\int_0^{2\pi}\tilde{\mathcal{H}}_{0n}\,dl,$$

$$\mathcal{W}_n=w^{-1}\int(\tilde{\mathcal{H}}_{0n}-\mathcal{K}_n)dl.$$

In this manner the normalization is carried out straightforwardly. This transformation is not convergent in general, but in practice we truncate it at a certain order and the terms we take provide useful information about the original system. In this case, we compute the averaged Hamiltonian up to $M=2$, because at this order we have a finite number of equilibria in the reduced phase space, as we will see in Sec. IV. Thence, as a consequence of Morse theory,[22] higher orders in the averaged Hamiltonian do not alter the qualitative behavior of the reduced system.

As we have pointed out before, the presence of the axial symmetry, not only in the perturbation, but also in the unperturbed part of $\mathcal{H}$, allows the system to be reduced again. In contrast with the first reduction, this second one is singular, the twice-reduced space is not a smooth surface. Depending on the value of the z component of the angular momentum the shape of this phase space is either a double-pinched sphere (lemon), when $N=0$, or a single-pinched one (balloon), if $N\neq 0$, see Ref. 19.

Fixing a value for N and L, the double-reduced space (from now on we call it $\mathcal{T}$) is two-dimensional and is described by the three linearly independent invariants (τ_1, τ_2, τ_3), which are related to the nodal-Lissajous variables as follows:

$$\begin{aligned}\tau_1&=\tfrac{1}{2}w^2L^2s^2(4e^2-2s^2-e^2s^2+4ec^2\cos 2g\\ &\quad -e^2s^2\cos 4g),\\ \tau_2&=wL(2-s^2-es^2\cos 2g),\\ \tau_3&=-2w^2L^2e\,\eta s^2\sin 2g,\end{aligned}\tag{8}$$

where $c=N/G$, $s=\sqrt{1-c^2}$, $\eta=G/L$, and $e^2=1-\eta^2$. The inverse change reads as

$$\begin{aligned}\cos 2g&=\frac{2[\tau_1(wL-\tau_2)+(2wL-\tau_2)(\tau_2^2-wL\tau_2-2w^2N^2)]}{[\tau_1-\tau_2(2wL-\tau_2)]\sqrt{2\tau_1+\tau_2^2+(2wL-\tau_2)^2-4w^2N^2}},\\ \sin 2g&=\frac{\tau_3\sqrt{4wL\tau_2-2(\tau_1+\tau_2^2)+4w^2N^2}}{[\tau_1-\tau_2(2wL-\tau_2)]\sqrt{2\tau_1+\tau_2^2+(2wL-\tau_2)^2-4w^2N^2}},\\ G&=\frac{1}{2w}\sqrt{4wL\tau_2-2(\tau_1+\tau_2^2)+4w^2N^2}.\end{aligned}\tag{9}$$

TABLE I. Poisson brackets for the τ_i'. The τ_i' on the left must be put on the left side of the bracket, while the τ_i' on the top are placed on the right-hand side of the brackets.

$\{,\}$	τ_1'	τ_2'	τ_3'
τ_1'	0	$-\frac{2}{L}\tau_3'$	$-\frac{2}{L}(1-\tau_2')(\tau_2'-2\tau_2'^2+N'^2)$
τ_2'	$\frac{2}{L}\tau_3'$	0	$-\frac{2}{L}\tau_1'$
τ_3'	$\frac{2}{L}(1-\tau_2')(\tau_2'-2\tau_2'^2+N'^2)$	$\frac{2}{L}\tau_1'$	0

Note that the angles l and ν have been ''eliminated'' after the first and second reductions, respectively. The invariants τ_1, τ_2, τ_3 are constrained by: $2w|N|\leqslant\tau_2\leqslant 2wL$ and

$$\tau_1^2+\tau_3^2=(2wL-\tau_2)^2(\tau_2^2-4w^2N^2), \tag{10}$$

for each fixed value of L and N such that $|N|\leqslant L$. It is worth noting that Eq. (10) defines the shape of $\mathcal{T}$, a surface of revolution which is not differentiable when the second member of Eq. (10) has double roots. Once we have described the two steps of the reduction process we apply them to Hamiltonian (7).

Carrying the normalization procedure to second order, we obtain the following normalized Hamiltonian expressed in nodal-Lissajous variables:

$$\begin{aligned}\mathcal{K}=&wL+\frac{\delta(4-\delta)}{16}wLs^2(1+e\cos 2g)-\frac{3a_3^2L^2}{32w^4}\\&\times\{48-112s^2+50s^4+e^2(-8+72s^2+25s^4)\\&+5es^2[4(-2+5s^2)\cos 2g+5es^2\cos 4g]\}.\end{aligned}$$

Now, we apply the second reduction to $\mathcal{K}$ with the aim of making N an integral out of this process. We need to fix values for N and L, neglect the constant terms in $\mathcal{K}$, and express it in the invariants associated with the axial symmetry using formulas (8) and (9). The Hamiltonian we get is

$$\mathcal{K}=-\frac{\delta(4-\delta)}{16}\tau_2-\frac{3a_3^2}{16w^6}(16\tau_1+41\tau_2^2-112wL\tau_2). \tag{11}$$

At first glance, the parameters appearing in the problem are δ, a_3, w, L, and N [which appear in Eq. (10)]. However, some of them are redundant as is shown by introducing the dimensionless variables $(\tau_1',\tau_2',\tau_3')$ according to

$$\tau_1=4w^2L^2\tau_1',\quad \tau_2=2wL\tau_2',\quad \tau_3=4w^2L^2\tau_3',$$

as well as the dimensionless z component of the angular momentum $N'=N/L$ in such a way that $0\leqslant|N'|\leqslant 1$. These variables have the Poisson structure given in Table I.

After introducing the new variables into Hamiltonian (11), we obtain

$$\mathcal{K}=-\frac{wL}{4}\left[\frac{\delta(4-\delta)}{2}\tau_2'+\frac{3a_3^2L}{w^5}(16\tau_1'+41\tau_2'^2-56\tau_2')\right]. \tag{12}$$

At this point we note that the factor a_3^2L/w^5 is dimensionless because a_3^2L has dimensions of time^{-5}. Hence, we define a new dimensionless parameter $\alpha=3a_3^2L/w^5$, which indicates the ratio between the frequency of the unperturbed oscillator and the frequency induced by the sextupolar term. After this transformation and the corresponding rescaling in time, Hamiltonian (12) becomes

$$\mathcal{K}=\frac{\delta(4-\delta)}{2}\tau_2'+\alpha(16\tau_1'+41\tau_2'^2-56\tau_2'),$$

where $\mathcal{K}$ is dimensionless and contains all the dynamical information of system $\mathcal{H}$. We finish the simplifications by introducing the parameter $\gamma=\delta(4-\delta)/(2\alpha)$, which in fact accounts for the relative influence between the detuning and the sextupolar perturbation. The final Hamiltonian is given by

$$\mathcal{K}_d=\alpha(\gamma\tau_2'+16\tau_1'+41\tau_2'^2-56\tau_2'). \tag{13}$$

Hence, Hamiltonian (13) contains the relevant dynamical information of system $\mathcal{H}$, depending on the two parameters γ and N' [which appears in Eq. (10) after being expressed in the new variables].

The equation determining the reduced phase space in the dimensionless variables and parameters is

$$\tau_1'^2+\tau_3'^2=(1-\tau_2')^2(\tau_2'^2-N'^2). \tag{14}$$

Each point in the double-reduced phase space defined by Eq. (14) corresponds to a family of perturbed ellipses in the original phase space. The trajectories with the same energy and with the same third component of the angular momentum are all represented in the same balloon or lemon. As an advantage over the nodal-Lissajous variables, all kind of orbits for $\mathcal{H}$ are contained in $\mathcal{T}$. For instance, polar orbits $(N'=0)$ are represented in lemons. Rectilinear orbits $(G=0)$ correspond to the upper (non-negative) part of the meridian $\tau_3'=0$ in lemons. The singularity (0,0,0) represents the rectilinear orbit $x=p_x=y=p_y=0$. The other singular point (in lemons or balloons) (0,1,0) represents the family of equatorial orbits. In Fig. 1, we draw the projections of a balloon and a lemon onto the plane $\tau_3'=0$ with the location of some types of trajectories.

IV. EQUILIBRIA AND BIFURCATIONS

Taking into account the Poisson brackets between the variables we derive the equations of the motion,

$$\begin{aligned}\dot\tau_1&=\{\tau_1,\mathcal{K}_d\}=-\frac{2\alpha}{L}(82\tau_2-56+\gamma)\tau_3,\\ \dot\tau_2&=\{\tau_2,\mathcal{K}_d\}=\frac{32\alpha}{L}\tau_3,\\ \dot\tau_3&=\{\tau_3,\mathcal{K}_d\}=\frac{2\alpha}{L}[16N^2(1-\tau_2)+(82\tau_2-56+\gamma)\tau_1\\&\quad+16(1-3\tau_2+2\tau_2^2)\tau_2].\end{aligned} \tag{15}$$

Note that we have dropped the primes for the sake of simplicity.

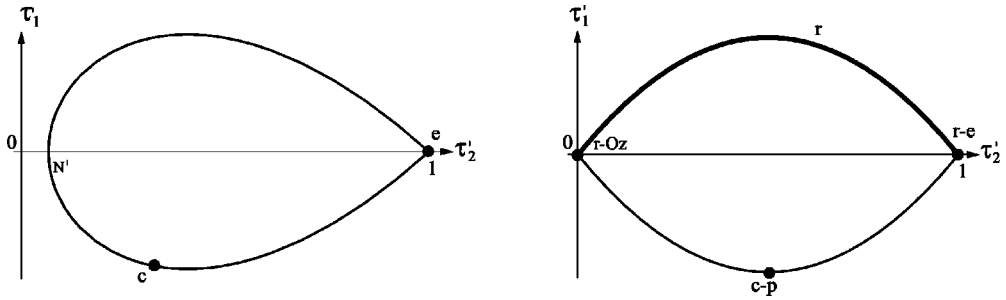

FIG. 1. Projections of a balloon and a lemon onto the plane $\tau_3'=0$, showing special types of trajectories. On the left-hand side, **c** stands for the family of circular orbits while **e** denotes the family of equatorial orbits. On the right-hand side, **r** represents the arc corresponding to rectilinear trajectories, while **r-Oz** are the trajectories in the *Oz* axis, **r-e** denotes rectilinear orbits on the equatorial plane and **c-p** are circular-polar trajectories.

A. Equilibria

The equilibria of the system are the local extrema of $\mathcal{K}_d$ on the semialgebraic variety (14). They are the roots of the system formed by the right-hand members of Eq. (15) equated to 0 together with the constraint (14).

From the second equation of (15), it follows that the equilibrium points are located on the plane $\tau_3=0$. Besides, the first equation also vanishes for $\tau_3=0$ and, from the third equation, the whole system vanishes if

$$\tau_1=\frac{16N^2(\tau_2-1)-\tau_2(2\tau_2^2-3\tau_2+1)}{82\tau_2-56+\gamma}, \tag{16}$$

provided $82\tau_2-56+\gamma\neq 0$. Finally, by substitution of (16) into (14) and making $\tau_3=0$, it follows that the coordinate τ_2 of the equilibria must satisfy the following polynomial equation:

$$\begin{aligned}(1-\tau_2)^2[&5700\tau_2^4+4(41\gamma-2040)\tau_2^3\\&+(2880-5700N^2112\gamma+\gamma^2)\tau_2^2-4N^2(41\gamma-2168)\tau_2\\&-N^2(3136+256N^2-112\gamma+\gamma^2)]=0,\end{aligned} \tag{17}$$

together with the restriction $|N|\leqslant\tau_2\leqslant 1$.

From Eq. (17) we observe that there always exists one equilibrium point, namely (0,1,0). Note that this point corresponds to a singular point of the variety (14), the only one if $N\neq 0$, and it accounts for equatorial orbits. The remaining equilibria are obtained from the real roots of the second factor of the polynomial Eq. (17) verifying $|N|\leqslant\tau_2\leqslant 1$. Being that this factor is a fourth degree polynomial it is possible to explicitly derive the coordinates of the equilibria. However, it is not easy to decide whether they are real or complex, as well as if they belong to the interval $[|N|,1]$. It is for this reason that we focus on the number of roots of this factor, rather than on the explicit expressions of them. In this way, if we denote by $\mathcal{P}(\tau_2)$ the fourth degree polynomial in Eq. (17), that is,

$$\begin{aligned}\mathcal{P}(\tau_2)=&5700\tau_2^4+4(41\gamma-2040)\tau_2^3+(2880-5700N^2\\&-112\gamma+\gamma^2)\tau_2^2-4N^2(41\gamma-2168)\tau_2\\&-N^2(3136+256N^2-112\gamma+\gamma^2),\end{aligned}$$

we have the following two basic results.

(i) The maximum number of equilibria is four.

Indeed, we have that $\lim_{\tau_2\to-\infty}\mathcal{P}(\tau_2)=+\infty$. On the other hand,

$$\mathcal{P}(0)=-N^2[256N^2+(\gamma-56)^2]<0 \quad (N\neq 0).$$

Thus, we can conclude that $\mathcal{P}$ always has a negative root for $N\neq 0$. Consequently, the number of roots in the interval $[|N|,1]$ is at most three and, hence, the total number of equilibria is at most four. (The case $N=0$ will be treated in detail in the following.)

(ii) The minimum number of equilibria is two.

This is a consequence of the Index Theorem.[23] We only need to realize that the Euler characteristic of the variety (14) is two and the indices of the equilibria must be 0, 1, or -1.

The key point now is to decide whenever the number of equilibria is two, three, or four depending on the values of the parameters γ and N; more specifically, according to the values of γ and N^2, since system (15) is symmetric with respect to the line $N=0$. A change in the number of equilibria implies a change in the number of real roots of $\mathcal{P}(\tau_2)$ in the interval $[|N|,1]$. This change is due to two different reasons. The first one is that one of the roots enters or leaves the interval taking the extreme values $|N|$ or 1, whereas the second is that two or more roots explode from a multiple root.

A root is located at the extrema of the interval $[|N|,1]$ if and only if one of the following equations are satisfied:

$$\begin{aligned}&\mathcal{P}(|N|)=-256N^2(1-|N|)^2=0,\\&\mathcal{P}(1)=(1-N^2)(420+52\gamma+\gamma^2+256N^2)=0.\end{aligned} \tag{18}$$

If we dispose of the case $|N|=1$ (the phase space gets reduced to a point) we find that along the curves $N=0$ and

$$A\equiv 420+52\gamma+\gamma^2+256N^2=0, \tag{19}$$

the polynomial $\mathcal{P}$ has a root located at the extrema of the interval $[|N|,1]$. Thus, a change in the number of equilibria is expected when crossing the line $N=0$ and when traversing A. On the one hand, due to the symmetry with respect to $N=0$, the crossing of $N=0$ does not mean a change in the number of equilibria. On the other hand, when the ellipse A is crossed the number of equilibria does change.

Now, we focus on the presence of a multiple root. To this end we consider the discriminant of the polynomial $\mathcal{P}$ which, after dropping constant factors, results in

$$\Delta(N^2,\gamma)=N^2(-840+3362N^2+71\gamma-\gamma^2)^2(-23\,887\,872\,000+151\,787\,520\,000N^2-280\,713\,600\,000N^4$$
$$+185\,193\,000\,000N^6+2\,786\,918\,400\gamma-10\,533\,888\,000N^2\gamma+10\,916\,640\,000N^4\gamma-133\,263\,360\gamma^2$$
$$+302\,630\,400N^2\gamma^2-97\,470\,000N^4\gamma^2+3\,340\,288\gamma^3-4\,245\,120N^2\gamma^3-46\,272\gamma^4+24\,012N^2\gamma^4+336\gamma^5-\gamma^6). \tag{20}$$

Thence, whenever $\Delta=0$, the polynomial $\mathcal{P}$ has a multiple root. Moreover, if given a root (N_0^2,γ_0) of Δ [i.e., $\Delta(N_0^2,\gamma_0)=0$] then, whether

$$\left.\frac{\partial\Delta}{\partial N^2}\right|_{N_0^2},\quad \left.\frac{\partial\Delta}{\partial\gamma}\right|_{\gamma_0}$$

do not vanish at the same time, the multiplicity of the root is two and is higher otherwise (see, e.g., for example, Ref. 24). This fact helps one to know the number of equilibria involved in the splitting of the multiple root.

The discriminant is made of the product of three factors (respectively, $\mathcal{F}_1$, $\mathcal{F}_2$, $\mathcal{F}_3$) and hence, it vanishes whenever one of them is equal to 0. So we must consider the following three cases:

(1) $\mathcal{F}_1=0$. This case is special because the variety of the corresponding phase space now has the aspect of a double-pinched sphere rather than a single-pinched one. Besides, along the line $N=0$, $\tau_2=0$ is a root of the polynomial $\mathcal{P}$. That is to say, the point (0,0,0) is an equilibrium point and it coincides with the other singular point of the semialgebraic variety (14) for $N=0$. In this manner, the singular points of the double reduced phase space are always equilibria. Besides, the polynomial $\mathcal{P}$ can be factorized as

$$(50\tau_2+\gamma-40)(114\tau_2+\gamma-72)\tau_2^2,$$

giving rise to three critical points in the lemons, namely

$$M_1\equiv(0,0,0),$$
$$M_3\equiv\left(\frac{(42+\gamma)(\gamma-72)}{12996},\frac{72-\gamma}{114},0\right),$$
$$M_4\equiv\left(\frac{(40-\gamma)(10+\gamma)}{2500},\frac{40-\gamma}{50},0\right).$$

Whereas M_1 exists independently of the value of γ, M_3 exists only if $\gamma\in[-42,72]$ and M_4 exists only if $\gamma\in[-10,40]$. Accordingly, the line $N=0$ can be divided in different segments where the number of equilibria change. Thus, we may conclude that for $\gamma\leqslant-42$ there are two equilibria; for $-42<\gamma<-10$ there are three equilibria; for $-10\leqslant\gamma<40$ there are four equilibria; for $40\leqslant\gamma<72$ there are three equilibria; for $\gamma\geqslant72$ there are two equilibria.

(2) $\mathcal{F}_2=0$. This case does not constitute an effective change in the number of equilibria. In fact, it arises from a symmetric configuration of the critical points with respect to the plane $\tau_1=0$. This is what happens when the denominator in Eq. (16), namely $82\tau_2+\gamma-56$, vanishes. Indeed, now the third equation in (15) becomes

$$\dot\tau_3=\frac{4}{68\,921}(26+\gamma)(-840+3362N^2+71\gamma-\gamma^2).$$

It vanishes at the same time as the second factor $\mathcal{F}_2$ of the discriminant. Being that $\tau_2=(56-\gamma)/82$, τ_1 is not longer determined by (16) but by (14) and, given τ_2, we find two different values for τ_1,

$$\tau_1=\pm(1-\tau_2)\sqrt{\tau_2^2-N^2}.$$

In this case the presence of a multiple root does not imply a change of the number of equilibria.

(3) $\mathcal{F}_3=0$. Identity $\mathcal{F}_3=0$ defines an algebraic curve in the plane (γ,N), symmetric with respect to the line $N=0$, made of two branches. Moreover, the first branch is defined for $\gamma\in(-\infty,40]$ while the second one is defined for $\gamma\in[72,\infty)$. We note that the curve is not defined for $\gamma\in(40,72)$, which corresponds with one of the segments obtained in the case $N=0$. We name this segment C.

Along $\mathcal{F}_3=0$ the polynomial $\mathcal{P}$ has a double root except for the values $(\gamma,N)=(40,0)$ and $(\gamma,N)=(72,0)$ where the root becomes triple. The goal now is to decide when the double root belongs to the interval $[|N|,1]$ or not. To this end we need to recall that a root enters or leaves the interval $[|N|,1]$ only if one of the lines A or $N=0$ is crossed. Thus, if along the branches of $\mathcal{F}_3=0$ the double root is outside (inside) the interval $[|N|,1]$ it will be so until one of the lines A or $N=0$ be crossed. One the one hand, the curve $\mathcal{F}_3=0$ intersects $N=0$ at the points (40,0) and (72,0). On the other hand, since the curve $\mathcal{F}_3=0$ and the ellipse A are tangent at the points $(-810/41,\pm(1425/1681)^{1/2})$, the branch defined for $\gamma\in(-\infty,40)$ is divided into two parts.

Take now this branch with $N\geqslant0$. For the part of it defined for $\gamma\in(-\infty,-810/41)$, the double root is bigger than 1. Thus, traversing this part of the branch does not imply a modification of the number of equilibria. Nevertheless, for the part of the branch defined for $\gamma\in[-810/41,40]$, which we call B, the multiple root is located in the interval $[|N|,1]$. Consequently, when crossing this part of the branch the number of equilibria changes. Finally, for the branch defined for $\gamma\in(72,\infty)$, the double root is negative and traversing this branch does not imply a change of the number of equilibria.

Taking into account the results obtained for $N=0$ and the curves A, B, and C, the parameter plane is divided into different regions where the number of equilibria can be determined (see Fig. 2).

B. Bifurcation lines and stability

As we have seen in Sec. IV A, there is a correspondence between the valid roots of the polynomial $\mathcal{P}$ and the number of equilibria. In this respect, the curves A, B and the segment

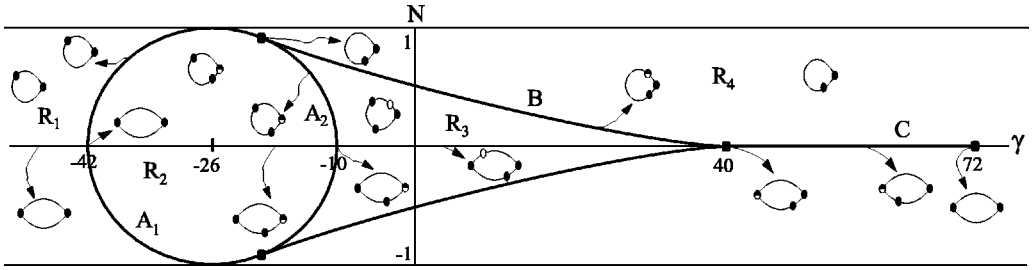

FIG. 2. Bifurcation diagram and meridian sections $\tau_3=0$ of balloons and lemons. Stable points (index=1) are characterized by a closed circle while unstable points with index-1 are by an open one and the ones with index 0 are represented by an open–closed circle.

C divide the parametric plane (γ,N) into several regions (R_1, R_2, R_3, R_4) for which the number of equilibria and, consequently, their stability change, see also Fig. 2. In other words, A, B, and C constitute the bifurcation lines of the problem.

In order to study the stability of the equilibria appearing in all regions of the parametric plane, we combine two techniques. On the one hand, for the equilibria appearing in the regular points of the balloons and lemons we use the standard method of Lagrange multipliers; on the other hand, the stability of the singular points can be deduced from the Index Theorem once the stability behavior of the regular equilibria has been established. Due to the complexity of a treatment for an arbitrary balloon or lemon (i.e., $N\in[-1,1]$ and $\gamma \in \mathbf{R}$), we accomplish the stability analysis of the problem fixing specific values of the parameters N and γ according to the different regions defined by the bifurcation lines. In this manner, we find the following.

(i) In regions R_1 and R_4 there are only two stable equilibria.
(ii) In region R_2 and on the segment C there are three equilibria: two stable and the other one unstable with index 0.
(iii) In region R_3 there are four equilibria: three of them with a stable character and the other one unstable with index equal to -1.

At this point, we are able to establish the type of bifurcation that takes place when lines A, B, or C are crossed. In this way, we detect the following four different bifurcations.

A *saddle-center* bifurcation takes place when passing from R_3 to R_4 (or from R_4 to R_3). In region R_3 there is a center and a saddle on the upper part of the balloon (and of the lemon) that come together at the bifurcation line B, giving rise to a degenerate point of parabolic type, and hence unstable. After crossing B, i.e., in zone R_4 of the parametric plane, the equilibrium disappears.

A *Hamiltonian flip* bifurcation occurs when traversing line A_1, that is, going from R_2 to R_1 or from R_2 to R_4 (and *vice versa*). What happens is that the (stable) singular equilibrium (0,1,0) in region R_1 (or in R_4), bifurcates when passing to R_2, losing its stability and giving rise to a new (stable) equilibria. Once in R_2 this point becomes a saddle and another center emerges from it at the lower part of balloons and lemons. Note that at A_1 the point (0,1,0) remains stable, as the index indicates. The Hamiltonian flip bifurcation is also called period doubling bifurcation as the usual scenario for it is that of a periodic orbit losing its stability, giving rise to a stable periodic orbit of twice the period, see Ref. 25. In Ref. 26 the terminology *subtle division* is used. See also Ref. 17 for a full analysis of the Hamiltonian flip bifurcation in a similar context to that studied here.

The passage from R_2 to R_3 or vice versa through the line A_2 undergoes another *Hamiltonian flip* bifurcation. Now, being in zone R_2, the point (0,1,0) is an unstable equilibrium of index 0 which splits into a center and a saddle once the curve A_2 is crossed. Specifically, in region R_3 there are four equilibria, three centers [one of them is the point (0,1,0)] and one saddle in the upper part of the balloons and lemons. After traversing A_2 the saddle and the center located at (0,1,0) meet in (0,1,0) forming an unstable equilibrium of index 0. Abraham and Marsden[26] term this bifurcation with the name of *murder*.

A *Hamiltonian Hopf* bifurcation occurs when the value $\gamma=72$ is reached while moving along $N=0$. This is a bifurcation of the equilibrium with coordinates (0,0,0). Indeed, the lemons with $\gamma\in[40,72)$ have three equilibria, two centers located at (0,1,0) and in the lower part of the lemon and one unstable point of index 0 placed at the origin. When $\gamma=72$ the center at the lower part of the lemon and the unstable equilibrium coalesce in (0,0,0) and become a center. This is the typical scenario of the Hamiltonian Hopf bifurcation, where two pairs of imaginary eigenvalues meet and split off the imaginary axis, forming a quartet $\pm\delta\pm i\epsilon$; see another example in Ref. 17.

Finally, the segment C corresponds to a bifurcation because there we find two centers and one unstable point whose index is 0 as it is detailed in the previous paragraph. Now, moving up and down to region R_4, the singular point at (0,0,0) disappears, but the two centers remain.

V. PHASE FLOW EVOLUTION

Complementary information about the dynamics of the system is obtained from the phase flow evolution. Since the reduced Hamiltonian $\mathcal{K}_d$ defines a dynamical system of one degree of freedom, we can obtain the trajectories, after fixing a value h of the energy, as the curves resulting from the intersections of the Hamilton function $\mathcal{K}_d=h$ with the surface (14), that is to say, they are the level curves of $\mathcal{K}_d=h$ on Eq. (14). This feature allows us to plot the phase flow of the system quite rapidly and accurately without even integrating

numerically the differential equations (15). In fact, we do not draw the level curves, but on the contrary we assign to every point on Eq. (14) the value that the Hamiltonian function $\mathcal{K}_d$ takes there. Hence, those points associated with the same value belong to the same level curve $\mathcal{K}_d = h$. This is the main idea of the technique known as *painting by number* (see Ref. 27).

Calculations involved to determine the phase flow are straightforward. First, we construct a two-dimensional grid which is orthographically projected on the lemons and balloons. Then, Hamiltonian $\mathcal{K}_d$ is evaluated at the corresponding points of Eq. (14) according to the grid we have chosen. Thereafter the resulting matrix is submitted as input to the commercial software *Transform*,[28] which computes and draws the level curves on the selected orthographic projection. This technique has been used to produce all the plots appearing in this section.

The phase flow is mainly commanded by the equilibria and their stability. Hence, making use of the conclusions arising from Sec. IV, we have studied the phase flow evolution choosing three ''representative'' paths on the parametric plane (γ, N) for which the stability and/or the number of equilibria change. Note that we only represent the phase flow for $N \geqslant 0$, as the parametric plane is symmetric with respect to the line $N = 0$. Moreover, note that the singular points of the double reduced phase space, i.e., the points of coordinates (0,0,0) and (0,1,0), are always equilibria. More precisely, the origin is a singular point of $\mathcal{T}$ only for $N = 0$ and we name it as M_1. For $N \neq 0$, we also denote by M_1 the equilibrium that for $N = 0$ is located at (0,0,0). On the other hand, (0,1,0) is always a singular point of $\mathcal{T}$ that we term by M_2.

Figure 3 shows the evolution of the system in phase space for $N = 0$ and $\gamma \geqslant 40$. For $40 \leqslant \gamma < 72$, there are three equilibria, namely, M_1, M_2, and M_3. Thus, it is easily concluded that the phase flow consists in rotations around the two centers M_2 and M_3. These rotations are split off by the separatrix passing through the point M_1 (equilibrium whose index is 0). As γ tends to the value 72, M_3 approaches M_1. Thus, when γ reaches this value, the equilibria M_2 and M_3 come together and a Hamiltonian Hopf bifurcation takes place. As a consequence, only M_1 and M_2 survive for $\gamma = 72$, and furthermore, M_1 becomes stable. This situation keeps on for $\gamma \geqslant 72$.

In Fig. 4 we present the phase flow evolution of the system along a path crossing the curve *B*. When $N = 0$ and $-10 < \gamma < 40$ (see Fig. 4 for $N = 0$ and $\gamma = 35$) we find the four equilibria: M_1, M_2, M_3, and M_4. A homoclinic loop (separatrix) asymptotic to the unstable equilibrium M_4, that surrounds M_1 and M_2, divides the phase space into three different zones of rotations around the stable equilibria M_1, M_2, and M_3. For $N \neq 0$ but still in region R_3 (see Fig. 4 for $N = 0.2$ and $\gamma = 15$), we encounter the same type of equilibria as in case $N = 0$ and $\gamma \in (10,40)$ and an equivalent phase flow structure. However, as we get close to the bifurcation curve *B*, the equilibria M_1 and M_4 begin to approach each other in such a way that when *B* is crossed, a saddle-center bifurcation occurs: the equilibria M_1 and M_4 meet at *B* and disappear once region R_4 is reached. Hence, for $N \neq 0$ and

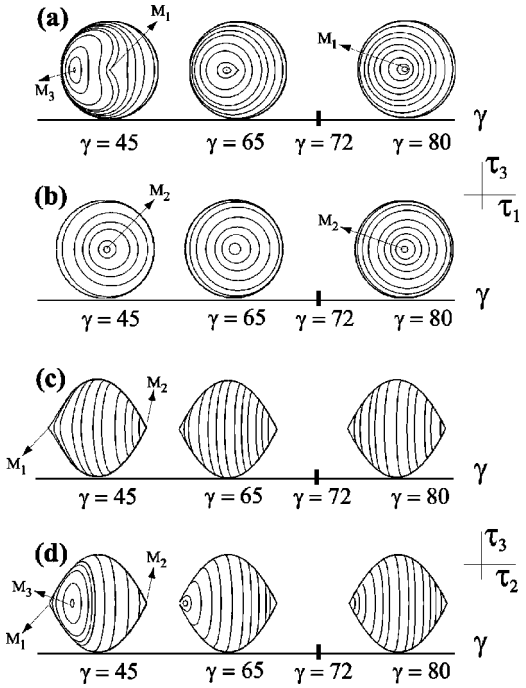

FIG. 3. Phase flow evolution of the system for $N = 0$ as the parameter γ increases from 45 to 80. Rows (a) and (b) correspond to ortographics projections onto the plane (τ_1, τ_3) viewed from $\tau_2 = 0$ and from $\tau_2 = 1$, respectively. Rows (c) and (d) correspond to ortographics projections onto the plane (τ_2, τ_3) viewed from $\tau_1 > 0$ and from $\tau_1 < 0$, respectively.

above the bifurcation curve (see Fig. 4 for $N = 0.2$ and $\gamma = 40$), the phase flow is made of rotations around M_2 and M_3. The sequence of plots finishes in the zone $N = 0$ and $40 < \gamma < 72$ (see Fig. 4 for $N = 0$ and $\gamma = 45$), where we find again the three equilibria M_1, M_2, and M_3, and whose phase flow structure has already been detailed. The appearance of M_1 obeys the presence of the singular point (0,0,0) for $N = 0$.

Finally, in Fig. 5 the evolution of the phase flow along a path traversing the line *A* is shown. The sequence starts inside the ellipse (see Fig. 5 for $N = 0.2$ and $\gamma = -15$). In this region (R_2) there are three equilibria, namely, M_1, M_2, and M_3. The phase flow consists of rotations around the stable equilibria M_1 and M_3. These rotations are split off by a separatrix passing through the third equilibrium M_2 whose index is 0.

Note that the ellipse can be crossed in two different ways: along a path crossing A_2, or along a path crossing A_1. When the ellipse is traversed in the first way (see Fig. 5 with $N = 0.2$ and $\gamma = -5$), M_2 undergoes a (murder) Hamiltonian flip bifurcation: from M_2 (which becomes stable) an unstable equilibrium named M_4 emanates. Now, a homoclinic orbit asymptotic to M_4 surrounds M_1 and M_2, and the corresponding phase flow has already been described. When the ellipse is crossed through A_1, the phase flow evolution is different. As we get close to the ellipse, M_3 approaches M_2 in such a way that when the ellipse is reached, they meet and, after crossing, only M_2 survives and it becomes stable. A (subtle division) Hamiltonian flip bifurcation has taken place, and the phase flow is simply made of rotations around M_1 and M_2 (see Fig. 5 for $N = 0.8$ and $\gamma = -5$).

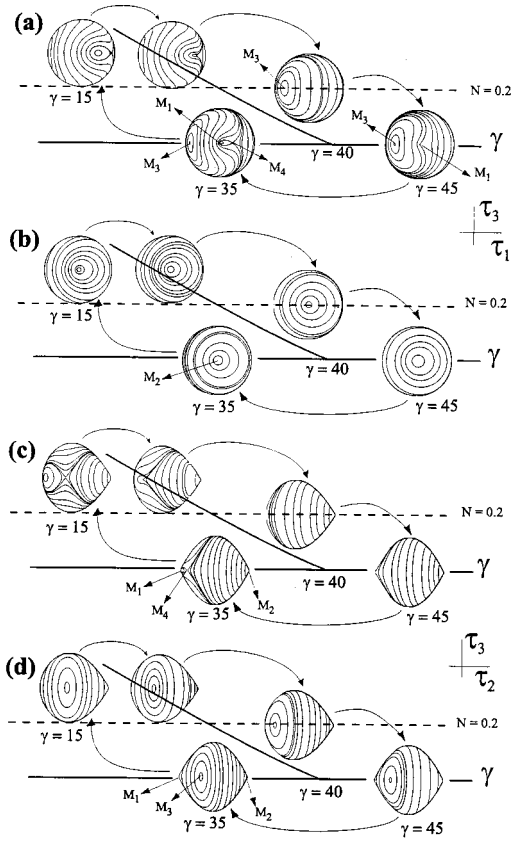

FIG. 4. Phase flow evolution of the system along a path crossing the saddle-center bifurcation curve. Rows (a) and (b) correspond to ortographics projections onto the plane (τ_1, τ_3) viewed from $\tau_2 = 0$ and from $\tau_2 = 1$, respectively. Rows (c) and (d) correspond to ortographics projections onto the plane (τ_2, τ_3) viewed from $\tau_1 > 0$ and from $\tau_1 < 0$, respectively.

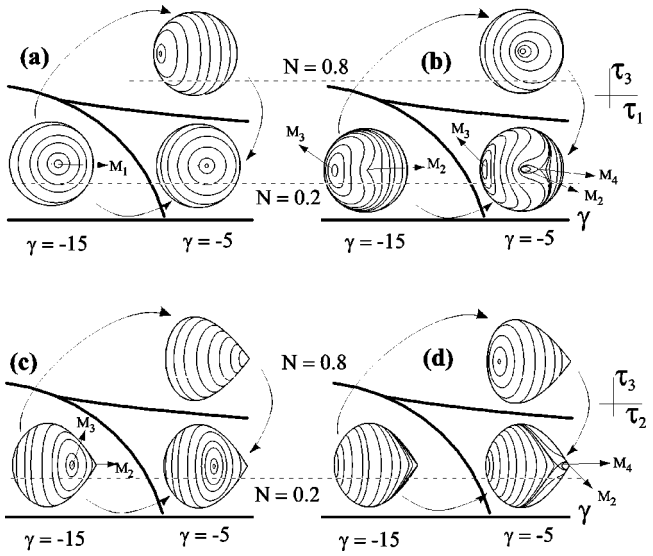

FIG. 5. Phase flow evolution of the system along a path crossing the bifurcation curves A_2 and B. Rows (a) and (b) correspond to ortographics projections onto the plane (τ_1, τ_3) viewed from $\tau_2 = 0$ and from $\tau_2 = 1$, respectively. Rows (c) and (d) correspond to ortographics projections onto the plane (τ_2, τ_3) viewed from $\tau_1 > 0$ and from $\tau_1 < 0$, respectively.

VI. CONNECTION TO THE ORIGINAL SYSTEM

A. Estimate of the error of the Lie transformation

The (formal and symplectic) change of variables Ψ constructed in Sec. III can be used to calculate an upper bound of the error committed in the truncation of the Lie transformation approach. Indeed, we start by calling $\mathbf{x}$ the set of variables (x, y, z, p_x, p_y, p_z) and $\mathbf{x}'$ the set of the transformed variables $(x', y', z', p_x', p_y', p_z')$.

Now we calculate the change $\mathbf{x}' = \mathbf{X}'(\mathbf{x}; \varepsilon)$. Note that $\mathbf{X}'$ is actually the change Ψ but written in Cartesian variables and gives explicit expressions of the new (transformed) variables $\mathbf{x}'$ in terms of the old (original) variables $\mathbf{x}$. Furthermore, we compute $\mathbf{x} = \mathbf{X}(\mathbf{x}'; \varepsilon)$ obtaining expressions of the old variables $\mathbf{x}$ as functions of the new variables $\mathbf{x}'$. At this step we have to mention that both $\mathbf{X}$ and $\mathbf{X}'$ are constructed by means of the generating function $\mathcal{W}$, expressed in Cartesians and using the formulas given in Ref. 14. Moreover both changes $\mathbf{X}$ and $\mathbf{X}'$ are built up to second order in the small parameter ε.

We can compose $\mathbf{X}$ with $\mathbf{X}'$ and compute explicitly the vector field $\mathbf{X}(\mathbf{X}'(\mathbf{x}; \varepsilon); \varepsilon)$, which must indeed be a second-order approximation to $\mathbf{x}$. Hence we arrive at

$$\|\mathbf{x} - \mathbf{X}(\mathbf{X}'(\mathbf{x}; \varepsilon); \varepsilon)\| = \varepsilon^3 E(\mathbf{x}) + \mathcal{O}(\varepsilon^4), \tag{21}$$

where $\|\cdot\|$ denotes the Euclidean norm in $\mathbf{R}^6$ and $E(\mathbf{x})$ is the global error term, which is obtained explicitly and depends on the three coordinates, their three conjugate moments, and the two significant parameters of the problem, say γ and α or, going back to the original Hamiltonian, the parameters a_3 and δ. Note that for this particular problem the parameter ε can be set equal to 1 as the real small parameters are inside the function E.

Now we have to bound the function E. Assuming that a_3 and δ satisfy $|a_3| \leqslant 5 \times 10^{-2}$ and $|\delta| \leqslant 3 \times 10^{-1}$, we have checked numerically that $|E(\mathbf{x})| \leqslant 5 \times 10^{-3}$ provided that $\|\mathbf{x}\| \leqslant 1.25$. This calculation shows the efficiency of the analytical approach, valid in a neighborhood of the origin of $\mathbf{R}^6$. Note that this result is in agreement with the values obtained after truncation of the Lie transformation at second order since $|E(\mathbf{x})|$ is of the order of $\mathcal{O}(\varepsilon^3)$.

Alternatively, one could obtain an equivalent estimate to Eq. (21) working with Hamiltonians. Indeed, composing Hamilton function (6) with the change Ψ truncated after second order, we have

$$|\Psi \circ \mathcal{H} - \mathcal{K}| < c\varepsilon^3,$$

with c a function depending on the nodal-Lissajous variables and on the parameters of the problem. After writing this estimate in Cartesian variables, one gets a similar expression to that obtained for $E(\mathbf{x})$. However, we have preferred to compose the change of variables instead of the Hamiltonians since the expressions involved in the process are shorter and therefore easier to be handled with the algebraic manipulator.

We end this section by mentioning that the validity of our Lie transformation (either in the form Ψ, $\mathbf{X}$ or $\mathbf{X}'$) is on a time scale $1/\varepsilon$. Nevertheless, other upper bounds of the time validity could be obtained based on Nehoroševv theory, see, e.g., Ref. 29, although this is outside the scope of the present paper.

B. Poincaré surfaces of section

We can validate the estimation of Sec. IV C by the analysis of the original Hamiltonian by means of the technique of Poincaré surfaces of section. To this end, it is convenient to express Hamiltonian (6) in cylindrical coordinates. In this way we obtain

$$\mathcal{H}=\frac{1}{2}(p_\rho^2+\rho_z^2)+\frac{p_\phi^2}{2\rho^2}+\frac{1}{2}(\rho^2+z^2) + \tfrac{1}{2}\delta z^2+a_3 z(2z^2-3\rho^2), \tag{22}$$

where $p_\phi=L_z$ is the z component of the total angular momentum and we have set $\omega=1$.

We describe the dynamics of the system by keeping $\mathcal{H}$, p_ϕ, and a_3 fixed and varying the detuning parameter δ. We will show that the behavior obtained with the surfaces of section is in very good agreement with the dynamics observed in the lemons and balloons in Sec. V.

For the sake of simplicity we focus on the case $p_\phi=0$ (e.g., $N=0$ in the reduced system), though analogous results can be shown for other values $|N|\geqslant 1$. For this case we define the surface of section as $\rho=0$, $p_\rho>0$. Under these conditions, the surface of section appears as a closed region in the plane (z,p_z) bounded by the curves

$$p_z=\pm\sqrt{2\mathcal{H}-(1+\delta)z^2-4a_3z^3}.$$

It is worth noting that the boundary of the section corresponds to a periodic rectilinear orbit, namely $\rho=0$.

We fix the energy $\mathcal{H}=0.75$. The reason is twofold: on the one hand the estimation of the error of the Lie transformation is satisfied; on the other hand we find a regular regime for all the values of the parameters that are considered. In addition we set $a_3=0.05$ as it is a small parameter and also in accordance with the estimation of the error. Taking into account the definition of the nodal-Lissajous variables and neglecting the contribution of the perturbative terms, we take $L\approx 0.75$ and thus

$$\gamma=\frac{\delta(4-\delta)}{6a_3^2L}\approx\frac{\delta(4-\delta)}{0.011\,25}.$$

So, fixed δ, a value of γ is obtained and we can compare the corresponding surface of section with the flow on the reduced phase space.

Figure 6 shows a sequence of surfaces of section for δ in the interval $[-0.06,0.22]$ that yields values of γ in $[-22, 74]$. We observe several fixed points on the surfaces of section that correspond to periodic orbits. To each periodic orbit we can associate a fixed point in the reduced phase space. Indeed, if we consider the case $\gamma=0$, we find five fixed points on the surface of section plus the boundary of the section. The periodic orbits are labeled as L_1, L_2 (rectilinear orbits), C_1, C_2 (almost circular orbits), and EQ (almost equatorial orbit).

We notice that the rectilinear polar orbit $\rho=0$ (the boundary of the surface of section) is associated with the equilibrium (0,0,0) on the lemon. The two rectilinear orbits L_1 and L_2 correspond to the unstable equilibrium M_4, whereas the almost circular orbits C_1 and C_2 correspond to the stable equilibrium M_3. Finally, the almost equatorial orbit EQ is related to the equilibrium (0,1,0) on the lemon. In this way, we find a direct connection between periodic orbits in the original system and critical points in the reduced phase space. Besides this remarkable connection we also observe the same qualitative evolution as γ increases. In fact, both the original and the twice-reduced system ($\mathcal{T}$) undergo the same sequence of bifurcations. Concretely, the Hamiltonian flip bifurcation in balloons and lemons turns to be a pitchfork bifurcation in the surfaces of section. This is due to the 2:1 covering of the twice-reduced phase space (see Ref. 17). Moreover, the Hamiltonian Hopf bifurcation remains the same in both the surfaces of section and the lemons and balloons.

It is interesting to mention that the values of γ for which the bifurcations are observed in the sequence of the Poincaré surfaces of section are in very good agreement with the values of γ for the bifurcation lines obtained in Sec. IV ($\gamma=-10,\gamma=40,\gamma=72$).

C. Dynamics of the full system: KAM theory

Since the normalized Hamiltonian $\mathcal{K}$ has been obtained after two reduction procedures (the second-order normalization followed by the exact axial-symmetry reduction), we have to attach a 2D torus to any point of the reduced phase space $\mathcal{T}$. More concretely, if $|N|<G<L$, i.e., when the nodal-Lissajous variables are well defined, the 2D tori are parametrized by the angles l and ν. (However, in case of equatorial or circular trajectories it is still possible to define other action-angle variables and perform the reconstruction of the invariant manifolds similarly.)

In particular one should speak of families of 2D tori depending on the parameters L and N. This means that equilibrium points on the balloons and on the lemons must be understood as invariant 2D tori in $\mathbf{R}^6$. Moreover they enjoy the same type of stability whenever all the eigenvalues of the linearization of each equilibrium have non-null real part. One can even compute explicit formulas of the (truncated) invariant 2D tori using the direct change of the Lie transformation. Notice that a second-order theory has been enough to study the dynamics of the original problem, but the higher order we reach with the Lie transformation process the more accurate the invariant manifolds of the original Hamiltonian we have encountered could be computed, provided that the global error after truncation will be maintained adequately.

In those equilibria of $\mathcal{T}$ where the linearization gives eigenvalues with null real part, a specific analysis should be performed. Nevertheless, in this problem such situations occur only on the bifurcation curves A, B and the point $(\gamma,N)=(72,0)$, which correspond, respectively, to Hamiltonian flip, saddle-center, and Hamiltonian Hopf bifurcations (note that this has been numerically verified in the latter subsection using the surfaces of section). For the analysis of these cases we refer to Refs. 17 and 19 where these bifurcations also occur. Hence, all the details about the reconstruction process can be followed in those papers. The bifurcations of relative equilibria are translated into bifurcations of 2D invariant tori or quasiperiodic orbits. Moreover the per-

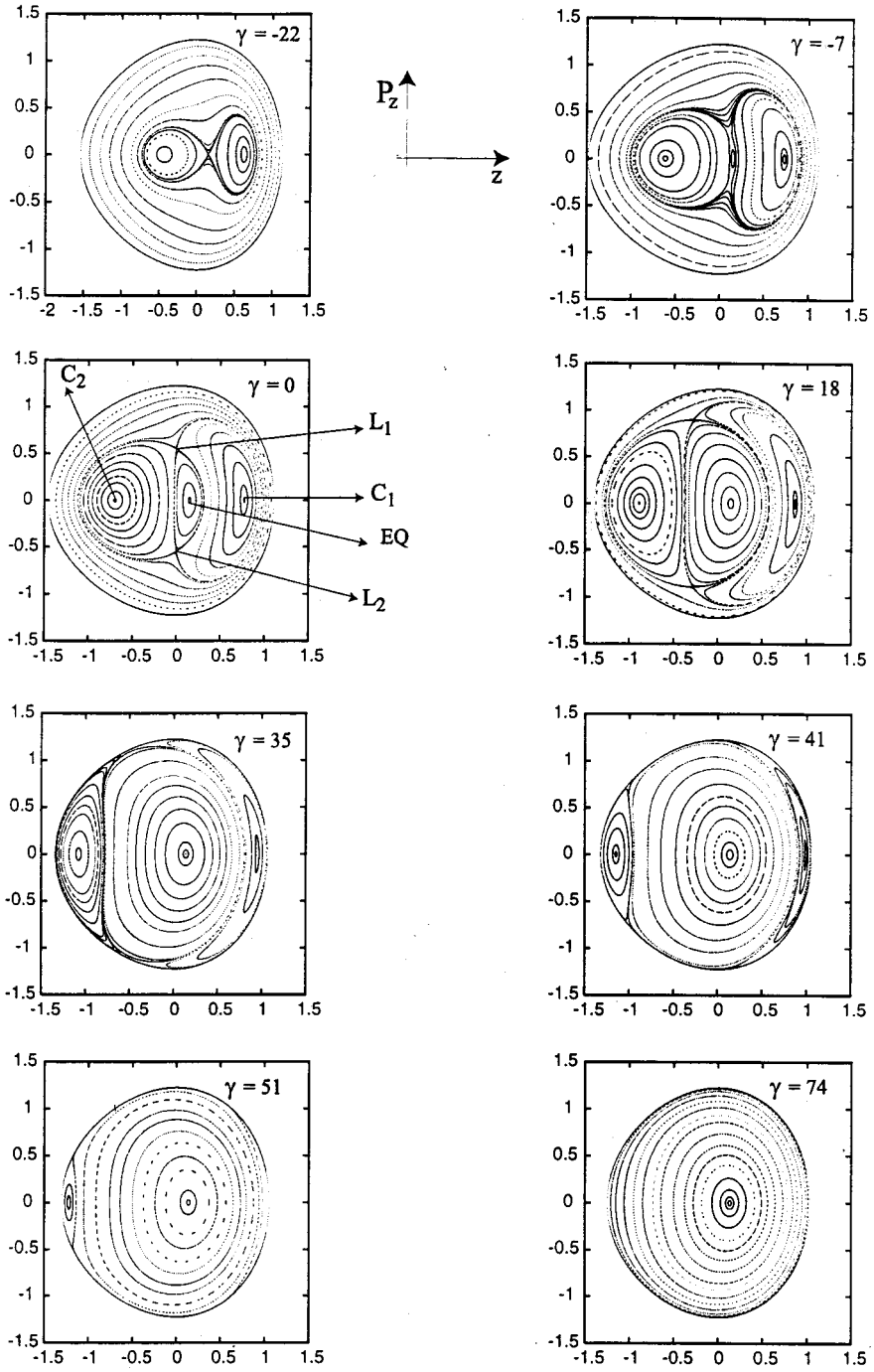

FIG. 6. Evolution of the Poincaré surfaces of section as a function of γ for a fixed energy $\mathcal{H}=0.75$, $p_\phi=0$, $a_3=0.05$.

sistence of these bifurcations is guaranteed by the estimate derived in Sec. VI A.

We do not give more details here about the reconstruction of the full system using KAM theory, as the analysis is analogous to the one performed in Refs. 17 and 19. Instead of that we have preferred to establish the connection to the original system by using the estimates of the error of the Lie transformation and the calculation of Poincaré surfaces of section.

D. Physical interpretation

From the physical point of view, a weakly perturbed ion trap is the most frequent situation encountered when working on trapping phenomena. In this sense, starting from a realistic model, this work provides a systematic study of the phase (orbit) space structure of a single ion trapped in a perturbed Penning trap.

In this paper we have shown that, for a fixed value of N, the dynamics is governed by the parameter which indicates the relative influence between the detuning δ and the sextupolar imperfection a_3. If we focus on the polar case $N=0$, which is the easiest to be achieved experimentally,[30] when γ goes from 0 ($\delta=0$) to $\gamma>72$ or to $\gamma<-42$, in both cases the phase space evolve to rotations around the stable equilibria M_1 and M_2 through several bifurcations. It is worth noting that this situation is equivalent to the one where the

sextupolar perturbation is not present ($a_3=0$). As for $a_3 \neq 0$ the system is integrable and the nonlinear character of the problem is provided by the sextupolar term. Thus, we can conclude that the presence of the detuning attenuates the nonlinear effects caused by the sextupolar perturbation. Taking into account that the value of the detuning can be controlled, this perturbative study can serve to decide which detuning added to the sextupolar perturbations would suppress the chaotic behavior induced by the sextupolar term when one treats the complete problem.

VII. CONCLUSIONS

We have shown that the sextupole approach to the Penning trap results in a generalization of the 3D Hénon–Heiles problem. Since the system is an axially symmetric perturbed harmonic oscillator, two reductions are made to get a one degree of freedom system. It is established that the phase space of the reduced system is a two-dimensional semialgebraic variety described by three linearly independent invariants. In this reduced phase space all kinds of perturbed ellipses of the original system are represented, avoiding the singularities introduced by other sets of variables.

A global analysis of the phase flow is made in terms of the two essential parameters of the problem. In this manner, the equilibria and their stability are determined, as well as the bifurcation lines in the parameter plane. It is worth noting that one of the essential parameters (N) accounts for the inclination of the perturbed ellipses. Thence, critical inclinations arise along the bifurcation curves in such a way that the stability of the family of orbits changes. These changes are produced mainly through three different types of bifurcations, the saddle-center bifurcation, the Hamiltonian Hopf bifurcation, and the Hamiltonian flip bifurcation.

The analysis derived through the paper indicates that the detuning parameter serves to prevent the appearance of separatrices, and therefore to attenuate the effects of the nonlinear chaotic dynamics.

ACKNOWLEDGMENTS

We acknowledge financial support from the Spanish Ministry of Education and Science (DGCYT Project Nos. ESP99-1074-C02-01 and PB98-1576) and from Universidad de La Rioja (Project Nos. API-98/A11 and API-99/B18).

[1] G. Contopoulos, ''A third integral of motion in a galaxy,'' Z. Astrophys. **49**, 273–291 (1960).
[2] V. Szebehely, *Theory of Orbits: The Restricted Problem of Three Bodies* (Academic, New York, 1967).
[3] G. Contopoulos, in *Stochastic Behavior in Classical and Quantum Hamiltonian Systems*, edited by G. Casati and J. Ford, Lecture Notes in Physics, Vol. 93 (Springer, Berlin, 1979).
[4] G. M. Zaslavski, R. Z. Sagdeev, D. A. Usikov, A. A. Chernikov, and A. R. Sagdeeva, *Weak Chaos and Quasi-Regular Patterns*, Cambridge Nonlinear Science Series, Vol. 1 (Cambridge University Press, New York, 1991).
[5] R. Dilão and R. Alves-Pires, *Nonlinear Dynamics in Particle Accelerators*, World Scientific Series on Nonlinear Science Series A, Vol. 23 (World Scientific, Singapore, 1996).
[6] H. Friedrich and D. Wintgen, ''The hydrogen atom in a uniform magnetic field: An example of chaos,'' Phys. Rep. **183**, 37–79 (1989).
[7] M. Gutzwiller, *Chaos in Classical and Quantum Mechanics*, Interdisciplinary Applied Mathematics, Vol. 1 (Springer, New York, 1990).
[8] F. M. Penning, ''Introduction of an axial magnetic field in the discharge between two coaxial cylinders,'' Physica (Amsterdam) **3**, 873–894 (1936).
[9] H. Dehmelt, ''Experiments with an isolated subatomic particle,'' Rev. Mod. Phys. **62**, 525–530 (1990).
[10] P. K. Ghosh, *Ion Traps*, International Series of Monographs on Physics (Oxford University Press, London, 1995).
[11] M. Kretzschmar, ''Single particle motion in Penning trap: Description in the classical canonical formalism,'' Phys. Scr. **46**, 544–554 (1992).
[12] G. Zs. K. Horvath, J.-L. Hernández-Pozos, K. Dholakai, J. Rink, D. M. Segal, and R. C. Thompsom, ''Ion dynamics in perturbed quadrupole ion traps,'' Phys. Rev. A **57**, 1944–1956 (1998).
[13] M. Hénon and C. Heiles, ''The applicability of the third integral of motion: Some numerical experiments,'' Astron. J. **69**, 73–79 (1964).
[14] A. Deprit, ''Canonical transformations depending on a small parameter,'' Celest. Mech. **1**, 12–30 (1969).
[15] J. D. Jackson, *Classical Electrodynamics* (Wiley, New York, 1998).
[16] P. Yanguas, ''Integrability, Normalization and Symmetries of Hamiltonian Systems in 1-1-1 Resonance,'' Ph.D. thesis, Universidad Pública de Navarra, Pamplona, Spain, 1998.
[17] S. Ferrer, H. Hanßmann, J. Palacián, and P. Yanguas, ''On perturbed oscillators in 1-1-1 resonance: The case of axially symmetric cubic potentials,'' J. Geom. Phys. **40**, 320–369 (2001).
[18] F. Verhulst, *Nonlinear Differential Equations and Dynamical Systems* (Springer, Berlin, 1996).
[19] R. Cushman, S. Ferrer, and H. Hanßmann, ''Singular reduction of axially symmetric perturbations of the isotropic harmonic oscillator,'' Nonlinearity **12**, 389–410 (1999).
[20] S. Ferrer and J. Gárate, ''On perturbed 3D elliptic oscillators: A case of critical inclination in galactic dynamics,'' in *New Trends for Hamiltonian Systems and Celestial Mechanics*, edited by E. A. Lacomba and J. Llibre, Advanced Series in Nonlinear Dynamics, Vol. 8 (World Scientific, Singapore, 1996), pp. 179–197.
[21] S. Ferrer, J. Palacián, and P. Yanguas, ''Hamiltonian oscillators in 1-1-1 resonance: Normalization and integrability,'' J. Nonlinear Sci. **10**, 145–174 (2000).
[22] J. Milnor, *Morse Theory*, Annals of Mathematics Studies (Princeton University Press, Princeton, NJ, 1963), Vol. 51.
[23] P. A. Firbi and C. F. Gardiner, *Surface Topology* (Horwood, New York, 1991).
[24] I. M. Gelfand, M. M. Kapranov, and A. V. Zelevinsky, *Discriminants, Resultants, and Multidimensional Determinants*, Mathematics: Theory & Application Series (Birkhäuser, Boston, 1996).
[25] K. R. Meyer, ''Generic bifurcation of periodic points,'' Transp. Res., Part A **149**, 95–107 (1970).
[26] R. Abraham and J. E. Marsden, *Foundations of Mechanics* (Dover, Redwood City, CA, 1985).
[27] L. Healy and E. Deprit, ''Paint by number: Uncovering phase flows of an integrable dynamical system,'' Comput. Phys. **5**, 491–496 (1991).
[28] TRANSFORM (Fortner Research LLC, Sterling, VA 20164, 1996).
[29] F. Fassò and G. Benettin, ''Composition of Lie transforms with rigorous estimates and applications to Hamiltonian perturbation theory,'' ZAMP **40**, 307–329 (1989).
[30] M. Moore and R. Blumel, ''Quantum manifestations of order and chaos in the Paul Trap,'' Phys. Rev. A **48**, 3082–3090 (1993).